33rd Annual International Conference of the IEEE EMBS
Boston, Massachusetts USA, August 30 - September 3, 2011

Functional Connectivity in Vergence and Saccade Eye Movement Tasks Assessed using Granger Causality Analysis

Yelda Alkan, Tara L. Alvarez
Department of Biomedical Engineering
New Jersey Institute of Technology
Newark, NJ, USA

Suril Gohel, Paul A. Taylor, Bharat B. Biswal
Department of Radiology
University of Medicine and Dentistry of New Jersey
Newark, NJ, USA

Abstract—**Throughout the day, the human visual system acquires information using saccade and vergence eye movements. Previously, functional MRI (fMRI) experiments have shown both shared neural resources and spatial differentiation between these two systems. FMRI experiments can reveal which regions are activated within an experimental task but do not yield insight into how regions of interest (ROIs) interact with each other. This study investigated the number and direction of influences among ROIs using a Granger Causality Analysis (GCA)-- a statistical technique used to identify if an ROI is significantly influencing or 'connected' to another ROI. Two stimulus protocols were used: first, a simple block design of fixation versus random eye movements; and second, a more cognitively demanding task using random versus predictable movements. Each protocol used saccadic movements and was then repeated using vergence movements. Eight subjects participated in each of the four experiments. Results show that when prediction was evoked, more connections between ROIs were observed compared to the simple tracking experiment. More connections were also observed during the vergence prediction task compared to the saccade prediction task. Differences within the number of connections may be due to the type of oculomotor eye movements, as well as to the amount of higher-level executive cognitive demand.**

Keywords- saccades ; vergence ; fMRI ; GCA

I. INTRODUCTION

Conjugate and disconjugate eye movements acquire visual information. Saccadic eye movements are conjugate tandem ocular movements used, for example, while reading. Vergence eye movements are disconjugate and allow depth perception via inward (convergence) and outward (divergence) turning of the eyes [1].

Functional MRI measures metabolic changes and has been reported to be correlated to direct neural measurements [2, 3]. Variations in cerebral blood flow, blood volume and the concentration of deoxyhemoglobin are the main parameters that form the blood oxygenation level dependent (BOLD) signal acquired during fMRI studies [4, 5]. Granger Causality Analysis [6] is a multivariate, data driven, time-dependent technique which has been used to assess effective and directional connectivity. [7-9] This statistical approach corresponds to neural connectivity between selected regions of interest (ROIs) [10-12].

The aim of this fMRI study was to compare saccade and vergence neural resources and to shed light on the dynamical Granger causal relationships for selected ROIs. We used a simple tracking task and a more cognitively demanding task to: 1) investigate if saccade and vergence systems share similar activation sites; 2) compute the flow of directional influences for selected ROIs; and 3) compare differences between the number of directed influences or 'connections' within and between saccadic and vergence experimental tasks.

This research is supported in part from an NSF CAREER BES-0447713 to TLA and NIH 5R01NS049176 to BBB

II. METHODOLOGY

A. Subjects

Eight volunteers (5 females, 3 males, mean age 26 ± 4 years) participated in this investigation. All subjects signed written consent forms approved by the University of Medicine and Dentistry of New Jersey and the New Jersey Institute of Technology Institution Review Boards. None of the subjects had neurological dysfunction. All subjects had normal binocular vision assessed using a Randot stereogram, near point of convergence and positive fusional ranges, described using methods in our prior study. [13]

B. Materials and Apparatus

A 3.0 Tesla Siemens Allegra MRI scanner with a standard head coil (Erlengten, Germany) was used to acquire brain images. Nonferrous light emitting diode (LED) targets (10 cm in height and 2 mm in width) were used for the visual stimuli. An infrared (λ = 950 nm) limbus tracking system manufactured by Skalar Iris (model 6500, Delft, Netherlands) with ±25° linear range recorded each subject's eye movements prior to the imaging session.

C. Functional Experimental Design

The LED visual line stimulus was viewed through the use of a mirror. Figure 1 (plot A1) shows the appearance of saccadic visual stimuli in three locations: 1) 0° (target along midline); 2) 10° into the left visual field or 3) 10° into the right visual field. Vergence visual stimuli were located at 2°, 3°, 4° combined vergence demand (Figure 1, plot A2).

A standard block design was used for each stimulus protocol. Saccade and vergence eye movements were evoked during alternating phases of "on" and "off" using different tasks shown in Figure 1, plot B. During the "on" phase, the visual step stimulus appeared for a random duration of time between 0.5 to 3.0 seconds. During the "off" phase, and the subjects were asked to fixate on one LED target. This was a simple oculomotor tracking experiment where each phase was 20 seconds. Since prediction is a more cognitive demanding task than the fixation versus random task, each phase for the prediction experiment was 40 seconds in duration. During random tracking, the subject was asked to look at the LED which was illuminated, and both the sequence and duration were random. During the predictable task, the subject could easily learn the sequence and each visual target was sequentially illuminated for 2 seconds.

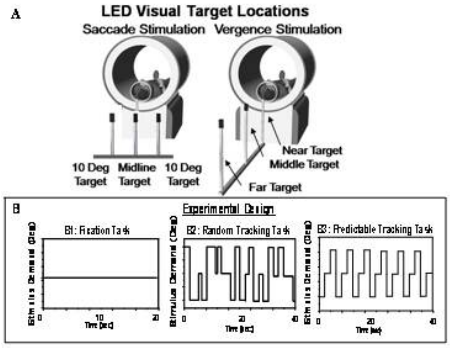

Figure 1: Experimental Design and Set-up.

D. Image Instrumentation and Procedure

Images were acquired with a T2* weighted echoplanar imaging (EPI) sequence. The imaging parameters were: FOV = 220 mm, 64 x 64 matrix, TR = 2000 ms, TE = 27 ms and flip angle = 90°. A total of 32 slices were collected in an axial configuration where each slice was 5 mm thick. Hence, the resolution was 3.4 x 3.4 x 5 mm resolution.

The functional imaging was followed by an MPRAGE (magnetization-prepared rapid gradient echo) scan to obtain high resolution anatomical images. The imaging parameters of the MPRAGE scan were: 80 slices, FOV = 220 mm, slice thickness = 2 mm, TR = 2000 msec, TE = 4.38 msec, T1 = 900 msec, flip angle = 8º, and matrix = 256 x 256 for a spatial resolution of 0.9 x 0.9 x 2 mm.

E. Data Analysis

1) Image Processing by AFNI

Data were analyzed using the AFNI software suite. Registration and motion correction were applied to the datasets. A minimum least square image registration method in AFNI was utilized for detection and correction of any motion-induced changes on the 3D image space. Motion correction was followed by detrending of the data to eliminate linear drifts. All saccade and vergence trials were used because head motion artifacts within each plane and between planes were minimal. The largest average degree of rotation was 0.14 deg ± 0.13 deg and 0.17 deg ± 0.14 deg in the pitch direction for the saccade and vergence datasets respectively. The largest average amount of movement within a plane was 0.27 ± 0.19 mm and 0.29 ± 0.27 mm in the inferior to superior plane for the saccade and vergence datasets respectively. Both are substantially less than one voxel.

A general linear model was used to analyze the fMRI BOLD signal. Probabilistic independent component analysis available through the MELODIC software from FSL was used to calculate the independent signal sources. A data driven independent component analysis (ICA) was used to extract a reference vector that contained the hemodynamic response and had the greatest correlation (Pearson's correlation coefficient) with the experimental block design. [14-16]

The anatomical and functional data were normalized to the standard Talairach-Tournoux coordinate space. The combination of individual voxel probability threshold and the cluster size threshold (11 voxels rounded to a volume of 650 mm^3 for our data set) yielded the equivalent of a whole-brain corrected for multiple comparison significance level of $\alpha < 0.001$. The cluster size was determined using the AFNI AlphaSim program, [17] which estimates the overall significance level by determining the probability of false detection through Monte Carlo simulation. Our simulation used 10,000 Monte Carlo iterations, assumed a cluster connection of the nearest neighbor, voxel dimension of 3.4 x 3.4 x 5 mm and sought a significance level of 0.001. Hence, a cluster size of 650 mm^3 or greater corresponded to $p < 0.001$ corrected for multiple comparisons. This combination of cluster size and correlation determined the regions of interest (ROIs) for this study.

Individual maps of t-statistics were smoothed with a Gaussian kernel of 6 mm full-width, half-maximum to account for inter-individual anatomical variation. [18-20] The functional data were displayed as z-scores, shown in the Figure 3 scale bar. The skull was removed since it is not relevant to our experiment.

Functional activation was located both bilaterally and on midline. The number of significant ROIs differed between the saccade and vergence datasets. For the saccadic dataset, the declive of the cerebellum was activated along the midline, whereas for the vergence dataset, the declive was activated bilaterally. Hence, we have chosen to analyze the cerebellum within the vergence dataset as two ROIs. For the saccade dataset the cerebellum was defined as a single ROI. A general linear model (GLM) analysis resulted in 19 ROIs for the saccade dataset and 20 ROIs for the vergence dataset.

2) Granger Causality Analysis

Granger Causality Analysis (GCA) is a statistical approach which is used to evaluate influences or effective 'connections' between neural regions. Granger-Causality assesses the F-statistics of the time series from fMRI data to quantify the existence of possible causal relationships between the ROI time series in terms of 'lags' or 'time separated values'. The residual variance in the full autoregressive model can be estimated by the unrestricted equation below:

$$x(t) = c1 + \sum_{i=1}^{p} a(i)x(t-i) + \sum_{j=1}^{p} b(j)y(t-j) + u(t) \quad (1)$$

$x(t)$ and $y(t)$ are two different time series to be evaluated for the causality interaction; t is the current time point; $a(i)$ and $b(j)$ are the linear prediction coefficients for x and y ; u is the residual error of the fit; and p is the lag length to be investigated. Using the F-test, the null hypothesis states that $b(j) = 0$ for all lags j (and therefore y does not influence or Granger-cause x) is tested. A similar test also can be applied to determine whether $x(t)$ causes (assessed using GCA) $y(t)$. [21] The residual variance from the above unrestricted equation is compared with the reduced autoregressive model, given by :

$$x(t) = c1 + \sum_{i=1}^{p} g(i)x(t-i) + e(t) \quad (2)$$

where $x(t)$ is the time series being evaluated for influence, t is the current time point, $g(i)$ is the linear prediction coefficient

for x; e is the residual or prediction error; and p is the lag length. [21, 22] The F-test comparison between these two models in Eqs. 1 and 2, full and reduced autoregressive, regarding residual variance can be calculated using Eq (3) below:

$$F_{y,x} = \frac{\left(\sum_{i=1}^{T} e\ (i)^{\ 2} - \sum_{i=1}^{T} u\ (i)^{\ 2}\right) \Big/ p}{\left(\sum_{i=1}^{T} u(i)\right)^{2} \Big/ (T - 2p - 1)} \qquad (3)$$

where T is the total number of time points and p is the length of lag. [22]

In our investigation, the ROIs were selected according to the functional activity calculated using a GLM analysis from both experimental tasks using vergence and saccade eye movements. Each ROI was masked to extract both an individual subject and group-level averaged time series. The extracted time series were used to create a Granger Causality matrix (GCM) for both an individual level and group-averaged level analysis. The GCM represents potential causal interactions between ROIs in terms of significance P-level values. The GCM were thresholded at P<0.05 with Bonferroni correction to calculate significant connections from all possible connections among ROIs. The best model order to calculate GCM was determined using the Bayesian Information Criterion (BIC) and Akaike Information Criterion for an fMRI dataset.[23] [12]

III. RESULTS

Typical eye movements are shown in Figure 2. Ensemble saccade and vergence responses are plotted as position (deg) versus time (sec). Saccadic eye movements are faster than vergence ones as shown in Figure 2 because the amount of time to acquire the target or reach steady state is less with saccade movements (left Figure 2) compared to vergence movements (right Figure 2). All subjects were able to perform the visual task in this study with ease.

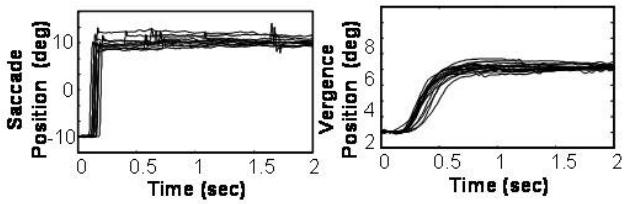

Figure 2: Ensemble saccade (left) and vergence (right) position traces (deg) as a function of time (sec).

The average functional activity from eight subjects is shown in Figure 3 for the random versus fixation (upper plots) and the prediction versus random movements (lower plots) for both saccadic and vergence eye movements. The significance of each pixel involved within the experiment task is shown with a color bar. ROIs were chosen from the observed functional activity in specific regions. GCA was applied within these ROIs.

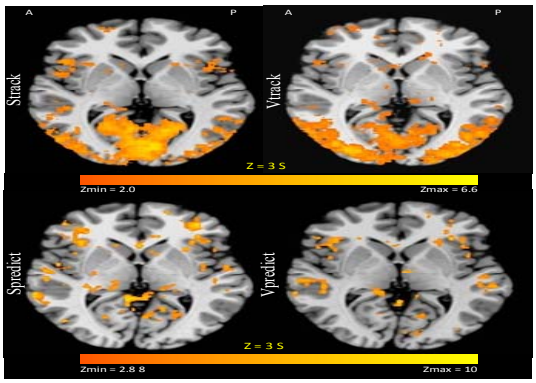

Figure 3: Average functional activity of saccadic and vergence eye movements.

The group-level GCA results are shown in Figure 4. There are a greater number of Granger causal connections during the prediction versus random tracking task compared to the simple fixation versus random tracking task, all of which have been thresholded at P< 0.05 with Bonferroni corrections. Figure 5 shows plots of the number of connections with one standard deviation for each group-level dataset. A repeated measures ANOVA shows that: there was a significant difference ($p < 0.0001$ and $F=92.4$) between prediction compared to the random tracking datasets while a trend was observed between the saccade prediction dataset compared to the vergence prediction dataset ($p = 0.07$ and $F = 4.8$). However, no statistically significant difference was observed between the saccade and vergence datasets from the random tracking experiments.

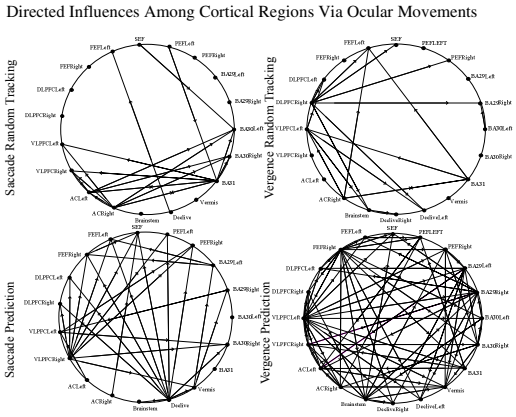

Figure 4: Directed influences among ROIs for saccadic and vergence eye movements .

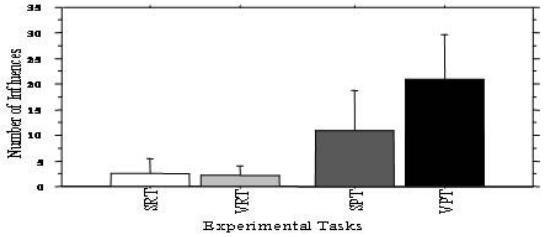

Figure 5: Number of GCA influences or effective 'connections' versus each experimental task. SRT: saccade random versus fixation task; VRT: vergence

random versus fixation task; SPT: saccade prediction versus random task; VPT: vergence prediction versus random task.

IV. Discussion

Differences in the group-level causal relationships for the selected ROIs using GCA within and between the saccade and vergence experimental tasks were observed. The differences in the number of influences may be due to the differences in cognitive demand between the tasks. We have shown that predictable eye movements occur earlier and with a greater peak velocity compared to movements evoked using random target. [24] GCA has also shown interregional temporal variability and interactions for regions that are functionally connected in memory and saccadic tasks.[22] [25]

The differences in regional connectivity or causal response observed within this present study may also be due in part to vasculature variations between different ROIs. [26] Lee and colleagues stated that larger vessels such as visible vessels and sulci require more blood which results in greater temporal delay when they are compared to vessels in the gray matter. Thus, this may lead to temporal variations in BOLD signals acquired from ROIs where the observed eye movement and task related differences results in different latency lags obtained from GCA. [26] Additionally, researchers hypothesized that the temporal variation observed within the inferior prefrontal regions and visual regions might be caused by the changes in hemodynamic response of different brain regions based on the underlying vasculature differences and the inability of fMRI resolution to capture such differences. [27] Therefore, more research is required to understand regional hemodynamic response and temporal variations in the BOLD signal between ROIs.

VI. Conclusion

The number of directed causal influences was estimated and compared within and between datasets using GCA. Results can be interpreted as eye movements that contain anticipatory behavior require more cognitive involvement than the simple random tracking experiments and / or physiological characteristics of the eye movements may affect interconnectivity within specific ROIs. While single cell recordings from primates and human case studies have reported numerous neural substrates participate in the generation of a saccade or vergence eye movement, the connectivity between these regions is still not fully understood. Recent reviews emphasize the need for more research to understand the directionality of communication and connectivity between ROIs for saccade[28] and vergence [29] movements. GCA has the potential to elucidate not only whether ROIs are connected but also the direction of information flow.

References

[1] J. Semmlow, *et al.*, "Short-term Adaptive Control Processes in Vergence Eye Movements," *Curr Psych Cog,* vol. 21, pp. 343-375, 2002.

[2] D. Attwell and C. Iadecola, "The neural basis of functional brain imaging signals," *Trends Neurosci,* vol. 25, pp. 621-5, Dec 2002.

[3] N. K. Logothetis and B. A. Wandell, "Interpreting the BOLD signal," *Annu Rev Physiol,* vol. 66, pp. 735-69, 2004.

[4] P. A. Bandettini, *et al.*, "Time course EPI of human brain function during task activation," *Magn Reson Med,* vol. 25, pp. 390-7, Jun 1992.

[5] K. K. Kwong, *et al.*, "Dynamic magnetic resonance imaging of human brain activity during primary sensory stimulation," *Proc Natl Acad Sci U S A,* vol. 89, pp. 5675-9, Jun 15 1992.

[6] C. W. J. Granger, "Investigating Causal Relations by Econometric Models and Cross-Spectral Methods.," *Econometrica,* vol. 37, pp. 424-38, 1969.

[7] M. L. Bagshaw, "Extension of Granger Causality in Multivariate Time Series Models Working Paper 8303," 1983.

[8] K. Friston, "Functional and effective connectivity in neuroimaging: a synthesis," *Hum. Brain Mapp.,* vol. 2, pp. 56-78, 1994.

[9] K. Friston, "BEYOND PHRENOLOGY: What Can Neuroimaging Tell Us About Distributed Circuitry? ," *Annu. Rev. Neurosci. ,* vol. 25, pp. 221-50, 2002.

[10] R. Goebel, *et al.*, "Investigating directed cortical interactions in time-resolved fMRI data using vector autoregressive modeling and Granger causality mapping," *Magn. Reson. Imaging* vol. 21, pp. 1251–1261., 2003.

[11] A. Roebroeck, *et al.*, " Mapping directed influence over the brain using Granger causality and fMRI," *Neuroimage* vol. 25, pp. 230–242, 2005.

[12] A. K. Seth, "Causal connectivity of evolved neural networks during behavior," *Network,* vol. 16, pp. 35-54, Mar 2005.

[13] T. L. Alvarez, *et al.*, "Vision therapy in adults with convergence insufficiency: clinical and functional magnetic resonance imaging measures," *Optom Vis Sci,* vol. 87, pp. E985-1002, Dec 2010.

[14] G. S. Berns, *et al.*, "Continuous functional magnetic resonance imaging reveals dynamic nonlinearities of "dose-response" curves for finger opposition," *J Neurosci,* vol. 19, p. RC17, Jul 15 1999.

[15] Calhoun, V.D. , *et al.*, "Modulation of temporally coherent brain networks estimated using ICA at rest and during cognitive tasks. ," *Hum Brain Mapp.,* vol. 29, pp. 828-38., 2008.

[16] M. Gavrilescu, *et al.*, "Functional connectivity estimation in fMRI data: influence of preprocessing and time course selection," *Hum Brain Mapp,* vol. 29, pp. 1040-52, Sep 2008.

[17] B. D. Ward, "Simultaneous Inference for FMRI Data. ," 2000.

[18] J. R. Binder, *et al.*, "Neural correlates of sensory and decision processes in auditory object identification," *Nat Neurosci,* vol. 7, pp. 295-301, Mar 2004.

[19] J. W. Lewis, *et al.*, "Distinct cortical pathways for processing tool versus animal sounds," *J Neurosci,* vol. 25, pp. 5148-58, May 25 2005.

[20] A. Schmid, *et al.*, "An fMRI study of anticipation and learning of smooth pursuit eye movements in humans," *Neuroreport,* vol. 12, pp. 1409-14, May 25 2001.

[21] Jeff B. Cromwell, *et al.*, *Multivariate Tests for Time Series Models*: Sage Publications, 1994.

[22] B. B. Biswal, *et al.*, "Task-dependent individual differences in prefrontal connectivity," *Cereb Cortex,* vol. 20, pp. 2188-97, Sep 2010.

[23] G. Schwartz, "Estimating the dimension of a model.," *The Annals of Statistics,* vol. 5, pp. 461-464, 1978.

[24] T. L. Alvarez, *et al.*, "Functional anatomy of predictive vergence and saccade eye movements in humans: a functional MRI investigation," *Vision Res,* vol. 50, pp. 2163-75, Oct 12 2010.

[25] K. Hwang, *et al.*, "Strengthening of top-down frontal cognitive control networks underlying the development of inhibitory control: a functional magnetic resonance imaging effective connectivity study," *J Neurosci,* vol. 30, pp. 15535-45, Nov 17 2010.

[26] A. Lee, *et al.*, "Discrimination of large venous vessels in time-course spiral blood-oxygen-level-dependent magnetic-resonance functional neuroimaging.," *Magn Reson Med,* vol. 33, pp. 745-54, 1995.

[27] R. Buckner, *et al.*, "Detection of cortical activation during averaged single trials of a cognitive task using functional magnetic resonance imaging.," *Proc Nat Acad Sci USA.,* vol. 93, pp. 14878-83., 1996.

[28] C. Pierrot-Deseilligny, *et al.*, "Eye movement control by the cerebral cortex," *Curr Opin Neurol,* vol. 17, pp. 17-25, Feb 2004.

[29] P. D. Gamlin, "Neural mechanisms for the control of vergence eye movements," *Ann N Y Acad Sci,* vol. 956, pp. 264-72, Apr 2002.